Clinical Cancer Research

Measurement of Tumor Antioxidant Capacity and Prediction of Chemotherapy Resistance in Preclinical Models of Ovarian Cancer by Positron Emission Tomography

Hannah E. Greenwood[1], Patrick N. McCormick[1], Thibault Gendron[2], Matthias Glaser[2], Raul Pereira[1], Oliver D. K. Maddocks[3], Kerstin Sander[2], Tong Zhang[3], Norman Koglin[4], Mark F. Lythgoe[1], Erik Årstad[2], Daniel Hochhauser[5], and Timothy H. Witney[1]

Abstract

Purpose: Drug resistance is a major obstacle for the effective treatment of patients with high-grade serous ovarian cancer (HGSOC). Currently, there is no satisfactory way to identify patients with HGSOC that are refractive to the standard of care. Here, we propose the system x_c^- radiotracer (4*S*)-4-(3-[^{18}F]fluoropropyl)-L-glutamate ([^{18}F]FSPG) as a non-invasive method to measure upregulated antioxidant pathways present in drug-resistant HGSOC.

Experimental Design: Using matched chemotherapy sensitive and resistant ovarian cancer cell lines, we assessed their antioxidant capacity and its relation to [^{18}F]FSPG uptake, both in cells and in animal models of human ovarian cancer. We identified the mechanisms driving differential [^{18}F]FSPG cell accumulation and evaluated [^{18}F]FSPG tumor uptake as predictive marker of treatment response in drug-resistant tumors.

Results: High intracellular glutathione (GSH) and low reactive oxygen species corresponded to decreased [^{18}F]FSPG cell accumulation in drug-resistant versus drug-sensitive cells. Decreased [^{18}F]FSPG uptake in drug-resistant cells was a consequence of changes in intracellular cystine, a key precursor in GSH biosynthesis. *In vivo*, [^{18}F]FSPG uptake was decreased nearly 80% in chemotherapy-resistant A2780 tumors compared with parental drug-sensitive tumors, with nonresponding tumors displaying high levels of oxidized-to-reduced GSH. Treatment of drug-resistant A2780 tumors with doxorubicin resulted in no detectable change in tumor volume, GSH, or [^{18}F]FSPG uptake.

Conclusions: This study demonstrates the ability of [^{18}F]FSPG to detect upregulated antioxidant pathways present in drug-resistant cancer. [^{18}F]FSPG may therefore enable the identification of patients with HGSOC that are refractory to standard of care, allowing the transferal of drug-resistant patients to alternative therapies, thereby improving outcomes in this disease.

Introduction

High-grade serous ovarian cancer (HGSOC) is a devastating disease with a 5-year survival rate of less than 42% (1). Despite initial rates of response to platinum-based chemotherapy of over 80%, the median progression-free survival is just 18 months (2, 3). Following first-line treatment, patients frequently relapse with platinum-sensitive disease. However, at each consequent relapse, the probability of response to further platinum-based treatment decreases (4), translating to a progressive decrease in effectiveness of platinum-based drugs. Clinically, response to platinum treatment in patients with ovarian cancer is measured as the length of time from treatment to relapse, known as the platinum-free interval (PFI; ref. 5). PFI, however, is a crude measure of drug sensitivity (6) and is particularly poor at predicting response for patients identified as "partially sensitive." These patients relapse 6 to 12 months after first-line treatment and will all subsequently receive further platinum-based treatment, despite benefit only being appreciable in 27% to 33% of cases (7). Better clinically-applicable biomarkers of platinum sensitivity in HGSOC are therefore urgently needed. The ability to identify patients refractive to the standard of care will enable the clinician to select the most appropriate second-line therapy for the individual patient, such as targeted therapy (e.g., PARP inhibitors) or biologics (e.g., bevacizumab).

Biochemical antioxidant mechanisms play a critical role in development of acquired drug resistance in cancer (8). Antineoplastic agents have been shown to produce oxidative stress in patients who receive these drugs, resulting in cell death in tumors sensitive to treatment (9–17). The plasticity of tumors, however,

[1]Centre for Advanced Biomedical Imaging, Division of Medicine, University College London, London, United Kingdom. [2]Department of Chemistry, Institute of Nuclear Medicine, University College London, London, United Kingdom. [3]Wolfson Wohl Cancer Research Centre, Institute of Cancer Sciences, University of Glasgow, Glasgow, United Kingdom. [4]Life Molecular Imaging GmbH, Berlin, Germany. [5]Cancer Research UK Drug-DNA Interactions Research Group, UCL Cancer Institute, University College London, London, United Kingdom.

Note: Supplementary data for this article are available at Clinical Cancer Research Online (http://clincancerres.aacrjournals.org/).

Corresponding Author: Timothy H. Witney, King's College London, 4th Floor, Lambeth Wing, St Thomas Hospital, London SE1 7EH, UK. Phone: +44 (0)20 7188 7188, Ext. 56327; E-mail: tim.witney@kcl.ac.uk

doi: 10.1158/1078-0432.CCR-18-3423

Translational Relevance

The majority of cancer deaths result from ineffective treatment of metastatic disease. Currently, there is no satisfactory way to identify patients that are refractive to the standard of care. PET imaging offers a potential solution to this clinical problem through the non-invasive assessment of molecular processes that underpin acquired drug resistance. The PET radiotracer (4*S*)-4-(3-[^{18}F]fluoropropyl)-L-glutamate ([^{18}F]FSPG) provides a surrogate marker of tumor antioxidant capacity through measurement of *de novo* glutathione biosynthesis. Elevated glutathione levels protect tumors from drug-induced oxidative stress, thereby conferring resistance. Here, we show that the magnitude of [^{18}F]FSPG accumulation in tumors can be used to predict drug resistance and subsequently monitor treatment efficacy in animal models of ovarian cancer. Given that [^{18}F]FSPG has already been used in pilot clinical trials, identification of drug resistance in patients may enable early intervention, potentially improving disease outcomes.

enables phenotypic adaptation to these oxidizing therapies, frequently mediated through the upregulation of glutathione (GSH), the body's most abundant antioxidant, in order to preserve cellular redox status and provide defense against reactive oxygen species (ROS) that are produced under conditions of oxidative stress (18). Biopsy samples have shown GSH levels to increase up to 10-fold in ovarian tumors following development of resistance to alkylating agents compared with samples taken before treatment (19). Furthermore, modulators of GSH biosynthesis, such as buthionine sulfoximine (BSO), resensitize human ovarian tumors, and cell lines to conventional therapy (20–23), highlighting the importance of GSH in the protection against tumor cell death.

One of the key mediators of the cell's antioxidant response is the amino acid transporter system x_c^-, which provides intracellular cysteine for *de novo* GSH biosynthesis. System x_c^- is a sodium independent transporter which under normal physiological conditions permits the exchange of 1 molecule of extracellular cystine, the dimeric form of cysteine, for 1 molecule of intracellular glutamate (24). Intracellularly, cystine is rapidly reduced to cysteine, which due to its low intracellular concentration (40–50 μmol/L) is limiting for GSH synthesis (25). (4*S*)-4-(3-[^{18}F]fluoropropyl)-L-glutamate ([^{18}F]FSPG) is a fluorine-18–labeled glutamate derivative that is specifically transported across the plasma membrane by system x_c^- (26), allowing the non-invasive assessment of system x_c^- transporter activity. Given the overexpression of system x_c^- in a wide-range of tumor types, [^{18}F]FSPG has been investigated clinically to produce high tumor-to-background PET images in hepatocellular carcinoma (HCC), non–small cell lung cancer and intracranial malignancies (27–29). We have shown previously in preclinical models of HGSOC that [^{18}F]FSPG uptake is sensitive to an elevation in GSH biosynthesis following drug-induced oxidative stress (30). Given the causal link between the levels of GSH and tumor resistance to therapy, here we examined [^{18}F]FSPG uptake as a predictive marker of drug resistance in HGSOC prior to treatment and as a marker of response post therapy.

Materials and Methods

Cell culture

Parental wild-type (WT; 93112519), cisplatin-resistant (CisR; 93112517), and doxorubicin-resistant (DoxR; 93112520) A2780 human ovarian cancer cells (Sigma Aldrich Ltd.) were grown in RPMI1640 media (ThermoFisher Scientific; 21875091) supplemented with 10% FBS (ThermoFisher Scientific; 21875091) and 100 U/mL penicillin, 100 μg/mL streptomycin (Sigma Alrich Ltd.; P4333). Patient-derived PEO1, PEO4, and PEO6 human ovarian cancer cell lines (European Collection of Authenticated Cell Cultures; 10032308, 10032309, and 10032310) were cultured as above, supplemented with 10 mmol/L sodium pyruvate (Sigma; S8636). Cells were maintained at 37°C and 5% CO_2. Clinically-formulated cisplatin (1 μmol/L; TEVA UK Ltd.; 51642169) or liposomal doxorubicin (1.0 μmol/L; Doxil; Janssen-Cilag Ltd.; 668950) was added to the growth media of CisR and DoxR cells, respectively, every third passage. A2780 WT, CisR, and DoxR were purchased from an authenticated cell bank and kept within 10 passages of the original vial. Short tandem repeat profiling could not be performed with PEO1, PEO4, or PEO6 cells. Mycoplasma testing was performed on a monthly basis.

Drug sensitivity in cell culture

Growth inhibition following drug treatment was characterized using the Vybrant MTT Cell Proliferation Assay Kit (ThermoFisher Scientific; V13154), according to the manufacturer's instructions. In 96-well plates, A2780 WT, CisR, and DoxR cells (2,000 cells/well); and PEO1, PEO4, and PEO6 (5,000 cells/well) were treated with increasing concentrations of clinically-formulated cisplatin or liposomal doxorubicin, 24-hour post-seeding (0.01 to 400 μmol/L). Complete media containing no drug was used as a control. Absorbance was measured at $\lambda = 570$ nm using a Multiskan FC Absorbance Plate Reader (THERMO-LABSYSTEMS). Viable cells were calculated as a percentage of the control group treated with no drug. Dose–response curves were generated and from them EC_{50} values were determined using GraphPad Prism (sigmoidal dose–response, fixed slope; v.6.0).

Clonogenic assay

PEO1, PEO4, and PEO6 cells were seeded in 10-cm dishes at densities of 2×10^3, 2×10^3, and 1×10^4 cells in 10-mL media, respectively. Forty-eight hours post seeding, cells were treated with clinically-formulated cisplatin (0.02–2 μmol/L) for 72 hours. At 72-hour drug containing media was replaced with fresh growth media and colonies were left to grow for a further 7 days. Colonies were fixed and stained in 6.0% glutaraldehyde (Sigma; 340355) and 0.5% crystal violet (Sigma; C0775). Colonies which contained >50 cells were counted to determine the surviving fraction (SF), which was calculated by dividing the total number of colonies formed by the number of cells seeded, multiplied by the plating efficiency.

Detection of intracellular oxidative stress

ROS were detected in human ovarian cancer cell lines using the cell permeable fluorophore CellROX Orange (Invitrogen; C10443). A2780 WT, CisR, and DoxR were seeded in 6-well plates at a density of 5×10^5 cells per well in 2-mL media 24 hours prior to performing the assay. PEO1, PEO4, and PEO6 cells were seeded at densities of 2×10^5, 6×10^5, and 8×10^5 cells per well

(2-mL media), respectively, 48 hours prior to assay to ensure complete cell attachment. Fresh media supplemented with 2 mmol/L glutamine was added to each 6-well plate 1 hour before the experiment. A final concentration of 1 μmol/L CellROX Orange reagent was added to each well and incubated for 30 min at 37°C, protected from light. Cells were then washed with PBS, harvested using 0.05% trypsin-EDTA (Thermo Fisher Scientific; 25300062) and suspended in 1 mL of ice-cold Hanks balanced salt solution (ThermoFisher Scientific; 14025092). The cell suspension was passed through a 35-μm filter and kept on ice prior to analysis on a LSRFortessa X-20 flow cytometer (561 nm laser and 586/15 bandpass filter; BD Biosciences), with 20,000 single cell events recorded per sample. Laser power remained constant between matched cell lines but was adjusted for A2780 vs. PEO lines. Data were gated post-acquisition based on forward (FS) and side scattering (SS) profiles to include only single cell events and to exclude cellular debris.

Glutamate quantification

The glutamate concentration in cell lysates was determined using a Glutamate Colorimetric Assay Kit following the manufactures guidelines (Biovision; K629). Cells were seeded in 6-well plates for glutamate quantification at the densities described above. One hour prior to harvesting the cells, fresh media supplemented with 2 mmol/L glutamine was added to all wells. Following harvesting with trypsin, cells were washed 3 times with 1 mL of ice-cold PBS. After the final wash, cells were suspended in 200 μL of glutamate assay buffer and sonicated using 3 sets of 5, 1-second pulses, on ice. Lysates were then centrifuged at 15,000 × *g* for 10 minutes at 4°C and the supernatant taken for analysis. Total intracellular glutamate was normalized to protein concentration, determined using the Pierce BCA assay (ThermoFisher Scientific; 23225) according to the manufacturer's instructions.

Cystine measurements using LC/MS

Cells seeded in 6-well plates (specific densities stated above) were supplemented with fresh media containing 2 mmol/L glutamine and 200 μmol/L cystine for 1 hour. Briefly, following incubation, media samples were removed and diluted into 490 μL of ice-cold extraction solvent (v/v 50% methanol, 30% acetonitrile, and 20% deionized water). For intracellular cystine quantification, cells were subsequently washed 3 times with ice-cold PBS and lysed in an appropriate volume of ice-cold extraction solvent to ensure approximately 3×10^6 cells/mL were collected. Both media samples and cell lysates were centrifuged at 15,000 × *g* at 1°C for 10 minutes. The supernatants were subjected to LC/MS as previously described (30).

In vitro analysis of total GSH

Cells were seeded into 6-well plates as described above. Total GSH was determined using either a colorimetric (Cayman Chemical; 703002) or luminescent (Promega; V6611) assay kit. For luminescent-based GSH quantification, cells were washed in ice-cold PBS, lysed in assay buffer, and centrifuged at 15,000 × *g* at 4°C for 10 minutes. Five microliters of supernatant along with 5 μL of GSH standards (1–100 μmol/L) were added to white 96-well plates and total GSH determined according to manufacturer's instructions. For colorimetric quantification, cells were processed as above, and total GSH detected according to the manufacturer's guidelines. Total intracellular GSH was normalized to protein concentration.

Western blot analysis

Western blot analysis was carried out using an established experimental method (31), adapted for use with the iBind Flex system (ThermoFisher Scientific) for primary and secondary antibody immunoblotting. For cell lysate collection, cells were seeded in 6-well plates, as described above. Rabbit monoclonal antibodies against human xCT (Novus Biologicals; NB300-318), NRF2 (Cell Signaling Technology; 12721), GLS1 (Abcam; ab156876), GCL (Abcam; ab190685), ABCC2 (Cell Signaling Technology; 12559), ABCC6 (Cell Signaling Technology; 10666), ABCB1 (Cell Signaling Technology; 13342), and ABCG2 (Cell Signaling Technology; 42078) were used for cell lysate analysis. Rabbit anti-human NRF2, GCL, p53 (Cell Signaling Technology; 2527), caspase3 Cell Signaling Technology; 9915), and cleaved caspase-3 antibodies (Cell Signaling Technology; 9915) were used for tumor lysate evaluation (prepared as described below). Actin was used as a loading control for all experiments (Cell Signaling Technology; 4967), with an HRP-linked anti-rabbit IgG secondary antibody (dilution; Cell Signaling Technology; 7074S). All antibodies were used at a 1:1,000 dilution, except for the anti-rabbit secondary antibody, which was diluted 1:200.

Radiotracer production

Automated radiosynthesis of [^{18}F]FSPG was accomplished utilizing a Scintomics HBIII platform (Scintomics), according to a previously reported method (30). The decay corrected isolated radiochemical yield was 51 ± 3% (n = 6) after solid-phase extraction purification, the radiochemical purity of [^{18}F]FSPG was >98% and the molar activity of the tracer was 4.2 to 21.9 GBq/μmol when starting from 2 to 4 GBq of [^{18}F]fluoride. The total synthesis time, from [^{18}F]fluoride in water to end of reformulation, was approximately 2 hours. Clinical-grade [^{18}F]FDG was obtained from PETNET solutions.

Radiotracer uptake in cells

Cells were seeded at the appropriate density in 6-well plates (see above). For all cell uptake experiments, radiotracers were added at a concentration of 0.185 MBq/mL. Cell uptake was performed for 60 minutes at 37°C in fresh growth media, following a previously established method (32). Radioactivity in samples was expressed as a percentage of the administered dose per mg protein.

In vivo tumor models

All animal experiments were performed in accordance with the United Kingdom Home Office Animal (scientific procedures) Act 1986. A total of 5×10^6 A2780 WT and DoxR cancer cells in 100-μL Dulbecco's PBS were injected subcutaneously into female Balb/c nu/nu mice aged 6 to 9 weeks (Charles River Laboratories). Tumor dimensions were measured using an electronic caliper and the volume calculated using the following equation: volume = $[(\pi/6) \times h \times w \times l]$, where h, w, and l represent, height, width, and length, respectively. Tumor size was monitored daily and imaging studies took place when tumor volume reached approximately 100 mm^3.

MicroPET imaging studies

Static PET scans were acquired on a Mediso NanoScan PET/CT system (1–5 coincidence mode; 3D reconstruction; CT

attenuation-corrected; scatter corrected). Mice received a bolus intravenous injection of approximately 3.7 MBq of [^{18}F]FSPG through a tail vein cannula. Following a 40-minute uptake period, a PET scan was acquired for 20 minutes. Animals were maintained under isofluorane anesthesia (1.5%–2% in oxygen) at 37°C during radiotracer administration and throughout the scan. CT images were acquired for anatomical visualization (480 projections; helical acquisition; 50 kVp; 300 milliseconds exposure time). Following image reconstruction, (Tera-Tomo 3D; 4 iterations, 6 subsets; 0.4-mm isotropic voxel size), VivoQuant software (Invicro) was used to quantify radiotracer uptake. Tumor and hindlimb muscle volumes of interest were constructed from 2D regions drawn manually using the CT image as reference. Data were expressed as percent injected dose per milliliter of tissue (%ID/mL). Tumor-to-background ratios were calculated by dividing the tumor %ID/mL by the muscle %ID/mL.

In vivo Doxil treatment studies

For treatment response studies, mice bearing approximately 100 mm^3 size-matched A2780 DoxR tumors were treated by intraperitoneal injection with Doxil (10 mg/kg). A cohort of untreated mice bearing 100 mm^3 A2780 DoxR tumors were imaged as pretreatment controls. Twenty-four hours post injection (D1), Doxil-treated mice were imaged with [^{18}F]FSPG PET as described above. A second cohort of mice received a further 2 Doxil doses, 2 and 5 days after the initial dose. These mice were subsequently imaged with [^{18}F]FSPG PET 6 days following the initial Doxil treatment (D6).

Ex vivo tumor sample preparation

Immediately following sacrifice, tumor tissue was dissected, snap frozen in liquid nitrogen, and stored at −80 °C. For GSH and GSSG analysis, each tumor sample was split into 2 pieces, placed into lysis Matrix tubes containing 1.4-mm ceramic beads (MP Biomedicals; 116913050) and assay buffer (Promega) with or without *N*-ethyl maleimide (NEM; 1 mmol/L), respectively. For Western blot samples, tumor tissue was added to separate Matrix tubes containing 1.4-mm ceramic beads and RIPA buffer. Tumor samples were lysed by rapid shaking using a high-speed benchtop reciprocating homogenizer (Fastprep-24 Sample Preparation Instrument; MP Biomedicals). The lysates were centrifuged at 15,000 × *g* at 4°C for 10 minutes and the supernatant collected for analysis. For all *ex vivo* experiments, data were expressed per milligrams of protein.

Statistical analysis

All data were expressed as the mean ± 1 SD. Statistical significance was determined using ANOVA followed by *t* tests multiple comparison correction (Tukey method; GraphPad Prism v.6.0).

Results

Cell model characterization

To investigate the role of intracellular redox homeostasis on tumor response to treatment, we used 2 sets of matched human ovarian cell lines with varying levels of drug sensitivity. The A2780, CisR, and DoxR lines were established previously from chronic exposure of the drug-sensitive A2780 WT cells to increasing concentrations of either cisplatin or doxorubicin, respectively (33, 34). The cisplatin-sensitive PEO1 cell line was cultured from a patient with relapsed ovarian cancer 22 months after 5-fluorouracil and chlorambucil combination chemotherapy with cisplatin. The PEO4 cisplatin-resistant cell line was cultured from ascites taken from the same patient 10 months later after further progressive disease but prior to re-treatment with high-dose cisplatin. Finally, the PEO6 cell line was obtained from ascites a further 3 months later, after the patient failed to respond to high-dose cisplatin (35).

We initially verified drug response rates of the matched A2780 cell lines in culture. CisR cells displayed moderate sensitivity to cisplatin in comparison to WT cells, with an EC_{50} of 10.1 ± 0.3 μmol/L versus 0.8 ± 0.2 μmol/L, respectively ($n = 3$; $P < 0.0001$; Fig. 1A), confirming previously reported values (36). DoxR cells were resistant to prolonged exposure at high micromolar doxorubicin concentrations ($EC_{50} = 29 \pm 2.1$ μmol/L and 0.47 ± 0.03 μmol/L for DoxR and WT, respectively; $n = 3$; $P < 0.0001$; Fig. 1B), again confirming previous findings (36). Interestingly, CisR and DoxR cells were cross-resistant to doxorubicin and cisplatin, respectively, despite not having been exposed to these drugs—possibly highlighting a shared mechanism of resistance. The EC_{50} for cisplatin in PEO1 cells was 2.6 ± 0.85 μmol/L, with PEO4 cells exhibiting lowered sensitivity to cisplatin in comparison to PEO1 cells, with an EC_{50} value of 14 ± 5.3 μmol/L ($n = 3$; $P = 0.01$; Fig 1C). There was no significant difference in EC_{50} between PEO1 and PEO6 cells ($n = 3$; $P = 0.083$). However, the dose required to kill 90% of the cells was 3-fold higher for PEO6 (19 ± 4.8 μmol/L for PEO1 vs. 66 ± 35 μmol/L for PEO6; $n = 3$; $P = 0.04$), revealing a small subset of PEO6 cells to be highly resistant. Motivated by this, a clonogenic assay was used to further explore cisplatin resistance in these cell lines. PEO6 cell lines showed decreased sensitivity to 0.5 μmol/L cisplatin following treatment compared to PEO1 cells (SF = 0.78 ± 0.22 vs. 0.432 ± 0.02, $P = 0.04$, $n = 3$), with both PEO4 and PEO6 cell lines exhibiting improved survival following treatment with 2 μmol/L cisplatin (SF = 0.08 ± 0.04, 0.12 ± 0.04 and 0.005 ± 0.004 for PEO4, PEO6, and PEO1, respectively; $n = 3$; $P = 0.05$, PEO1 vs. PEO4; $P = 0.008$, PEO1 vs. PEO 6; Supplementary Fig. S1).

Drug-resistant ovarian cancer cells upregulate antioxidant defense mechanisms

We hypothesized that drug resistance in these cell lines was mediated, at least in part, by the upregulation of key antioxidant pathways. In support of this hypothesis, we found that basal intracellular ROS levels were decreased 24% in CisR ($P = 0.03$) and 86% in DoxR cells ($P < 0.0001$), compared with the WT parental cells ($n = 3$; Fig. 1D). Intracellular ROS in the PEO4 and PEO6 cell lines were also decreased 60% ($P = 0.02$) and 55% ($P = 0.03$), respectively, compared with PEO1 ($n = 4$; Fig. 1E). Accompanying this decrease in intracellular ROS, intracellular GSH was increased 1.8-fold in the CisR cells and 3.3-fold in DoxR cells, compared with WT cells ($n = 3$; $P = 0.04$, WT vs. CisR; and 0.0002, WT vs. DoxR; Fig. 1F), with GSH increased 2.7- and 3.8-fold in the PEO4 and PEO6 cells compared with PEO1 ($n = 3$; $P < 0.0001$, PEO1 vs. PEO4; and $P < 0.0001$, PEO1 vs. PEO6; Fig. 1G).

[^{18}F]FSPG, but not [^{18}F]FDG uptake predicts drug sensitivity in A2780 cells

We have previously shown that system x_c^- provides a functional readout of *de novo* GSH biosynthetic flux, which can be

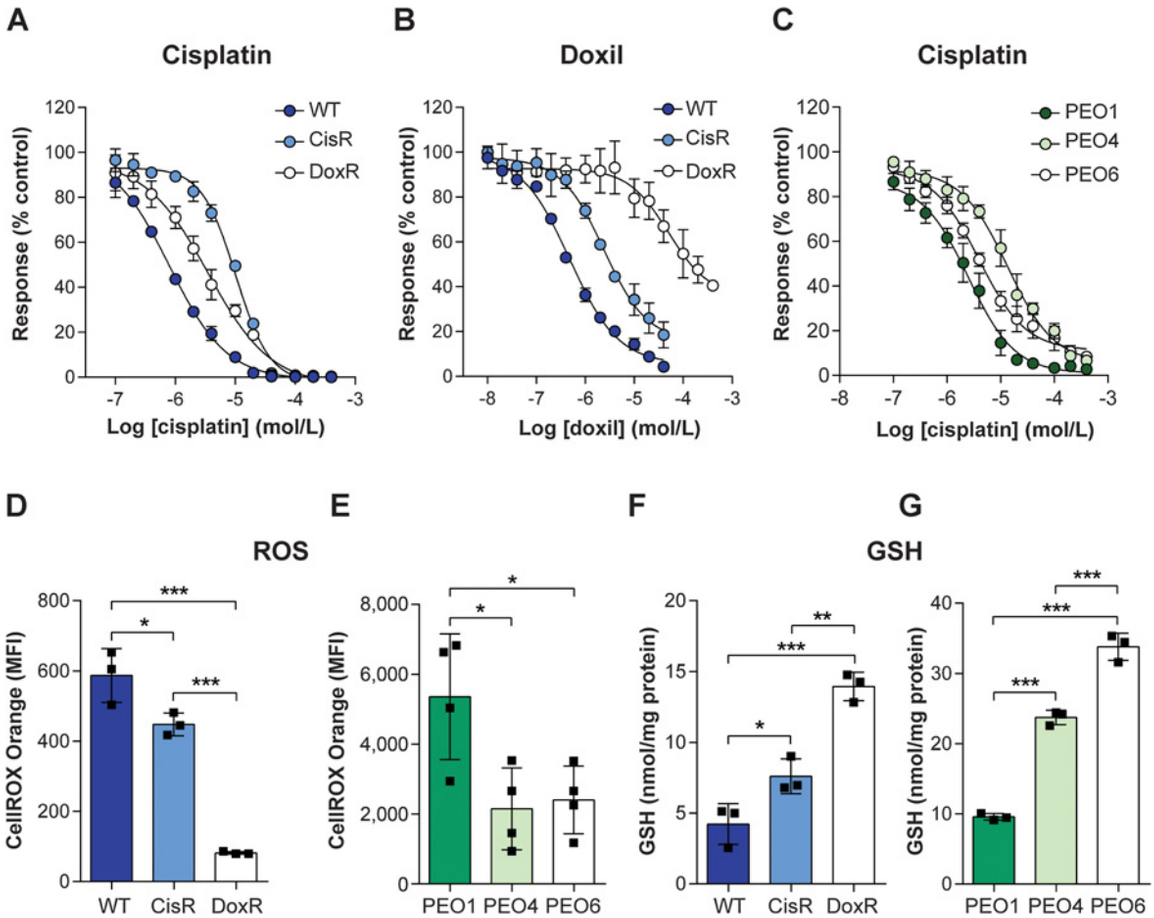

Figure 1.
Chemotherapy resistance accompanies protection against oxidative stress in human ovarian cell lines. Sensitivity of A2780 (**A** and **B**) and PEO cell lines (**C**) to treatment with cisplatin (**A** and **C**) or Doxil (**B**), as measured by an MTT assay. Data are expressed as a percentage response compared with untreated cells following 72-hour treatment ($n = 3$). **D** and **E**, Global levels of intracellular ROS in A2780 (**D**) and PEO (**E**) ovarian cancer cell lines, measured by flow cytometry. Different laser power was used for data acquisition of A2780 matched lines versus PEO. **F** and **G**, Intracellular baseline GSH levels in the drug-sensitive and drug-resistance A2780 (**F**) and PEO cell lines (**G**). Scatter plots represent individual biological repeats. *, $P < 0.05$; **, $P < 0.01$; ***, $P < 0.001$. MFI, median fluorescence intensity.

imaged non-invasively using [^{18}F]FSPG PET (30). Given that the rate of GSH biosynthesis may provide a surrogate marker of drug sensitivity, we next assessed system x_c^--mediated [^{18}F]FSPG uptake in drug-sensitive and drug-resistant ovarian tumor cells in culture. The molecular structure of [^{18}F]FSPG is shown in Fig 2A. In CisR cells, [^{18}F]FSPG accumulation was

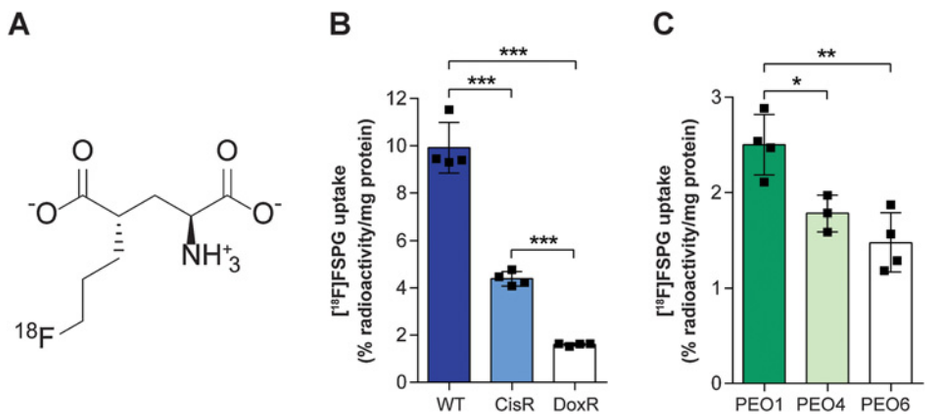

Figure 2.
[^{18}F]FSPG retention is decreased in drug-resistant cells. **A**, Molecular structure of [^{18}F]FSPG. **B** and **C**, [^{18}F]FSPG cell uptake and accumulation following 60-minute incubation in A2780 cell lines (**B**) and PEO cell lines (**C**). Scatter plots represent biological repeats performed in triplicate. *, $P < 0.05$; **, $P < 0.01$; ***, $P < 0.001$.

reduced by 57% compared to WT, falling from 9.9 ± 1.1% radioactivity/mg protein to 4.3 ± 0.3% radioactivity/mg protein ($P < 0.0001$). In the more resistant DoxR cells, [^{18}F]FSPG accumulation was 81% lower than WT (1.6 ± 0.1% radioactivity/mg protein; $n = 4$; $P < 0.0001$; Fig. 2B). [^{18}F]FDG is routinely used in the clinic for cancer diagnosis and staging. In contrast to [^{18}F]FSPG, there was no correlation between [^{18}F]FDG uptake and the magnitude of drug resistance (Supplementary Fig. S2), with [^{18}F]FDG cell uptake measured at 1.5 ± 0.2% radioactivity/mg protein, 10.6 ± 2.1% radioactivity/mg protein and 6.3 ± 1.1% radioactivity/mg protein, for CisR, DoxR, and WT, respectively ($n = 3$). Confirming findings in the A2780 cell lines, [^{18}F]FSPG uptake was decreased 29% and 41% in the more resistant PEO4 and PEO6 cell lines, compared with PEO1 cells (2.5 ± 0.3% radioactivity/mg protein, 1.8 ± 0.2% radioactivity/mg protein, and 1.5 ± 0.3% radioactivity/mg protein, for PEO1, PEO4, and PEO6, respectively ($n = 3$–4; $P = 0.03$, PEO1 vs. PEO4; and $P = 0.003$, PEO1 vs. PEO6; Fig. 2C).

Intracellular cystine is decreased in chemotherapy-resistant cells

System x_c^- is the key transporter used in tumor cells for the exchange of intracellular glutamate with extracellular cystine (Fig. 3A). The altered radiotracer flux through system x_c^- occurred in the absence of any changes in xCT protein expression, the transporter component of system x_c^-. Splice variants of glutaminase 1, the kidney-type glutaminase (KGA) isoform and the glutaminase C isoform (GAC), which provide intracellular glutamate through glutaminolysis, showed elevated expression in the CisR and DoxR resistant lines in comparison to WT (Fig. 3B). The PEO4 and PEO6 cell lines showed increased expression of the redox-sensitive transcription factor NRF2 and 1 of its downstream targets glutamate-cysteine ligase (GCL)—the rate limiting enzyme in GSH biosynthesis (Fig. 3B).

The absence of changes in [^{18}F]FSPG transporter expression motivated us to investigate the roles of intracellular concentrations of glutamate and cystine to determine their potential role in [^{18}F]FSPG retention. In the A2780 cell lines, there was no significant difference in the intracellular concentration of glutamate, despite the observed differences in glutaminase expression ($n = 3$; $P > 0.05$; Fig. 3C). In the PEO cell lines, however, there was a 54% decrease in intracellular glutamate for PEO4 cells and 40% in the PEO6 cells, compared with PEO1 ($n = 3$; $P = 0.005$, PEO1 vs. PEO4; and $P = 0.02$, PEO1 vs. PEO6; Fig. 3D). Additionally, intracellular cystine was decreased over 90% in the drug-resistant A2780 lines, compared with drug sensitive ($n = 3$; $P = 0.0019$, WT vs. CisR; and $P = 0.0021$, WT vs. DoxR; Fig. 3E). Markedly lower intracellular cystine was also measured in PEO4 and PEO6 cells compared

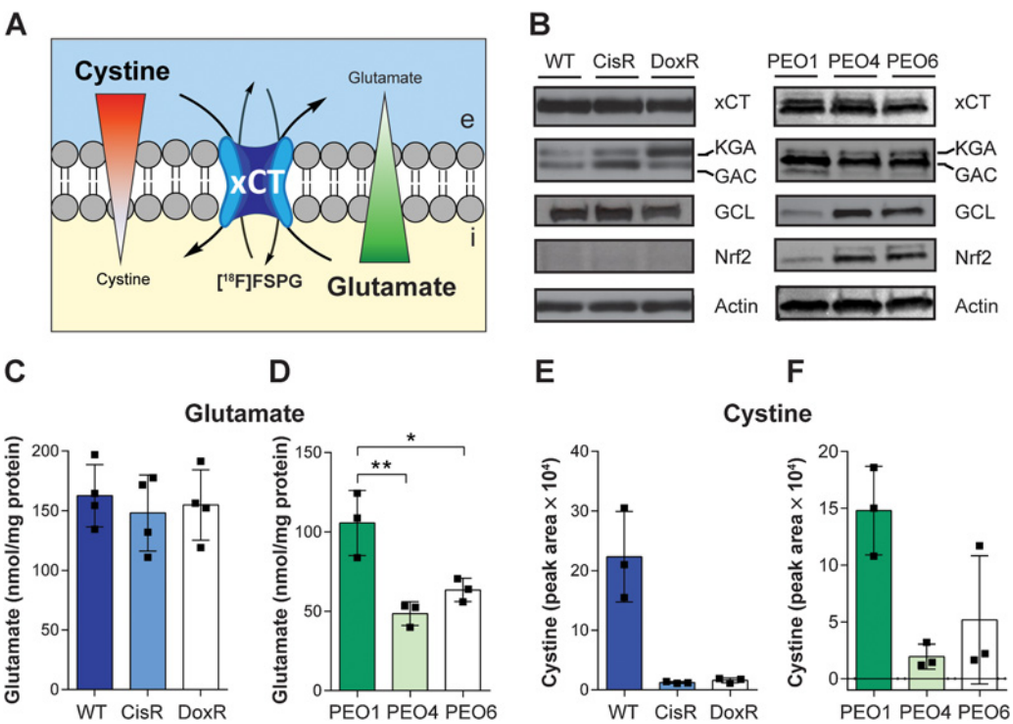

Figure 3.

Intracellular levels of cystine are decreased in drug-resistant cancer cells. **A,** Model of [^{18}F]FSPG accumulation, with mechanisms known to control radiotracer accumulation. Uptake of [^{18}F]FSPG is predicted to occur through exchange with intracellular glutamate, with efflux controlled by the exchange with extracellular cystine. Red and green triangles represent the concentration gradients of cystine and glutamate across the plasma membrane. e, extracellular; i, intracellular. **B,** Western blot analysis of the levels of xCT, glutaminase isozymes (KGA, kidney-type glutaminase; GAC, glutaminase-C), glutamate-cysteine ligase (GCL), and NRF2. Intracellular levels of glutamate (**C** and **D**) and cystine (**E** and **F**) in A2780 (**C** and **E**) and PEO human ovarian cancer cell lines (**D** and **F**). Data presented as mean with individual scatter plots representing independent experiments. *, $P < 0.05$; **, $P < 0.01$.

with PEO1s (86% and 65% decrease, respectively; $n = 3$; $P = 0.018$, PEO1 vs. PEO4; and $P = 0.059$, PEO1 vs. PEO6; Fig. 3F).

ABC transporter expression

ATP-binding cassette (ABC) transporter proteins play an important role in acquired drug resistance, facilitating the efflux of anticancer drugs, frequently as GSH conjugates (37). To explore the role of key ABC transporters and their potential link to the tumor antioxidant response, we examined their expression in our panel of ovarian cancer cells. In the DoxR cells, ABCB1 and ABCC2 was expressed to high levels, whereas functional expression of these transporters was absent in the WT and CisR lines. Conversely, ABCG2 expression was elevated in WT cells, with no expression observed in all other lines. The ABCC6 transporter was not expressed in any of the cell lines tested, with PEO1, PEO4, and PEO6 cells expressing neither ABCB1, ABCC2, ABCG2, nor ABCC6 (Supplementary Fig. S3).

[18F]FSPG uptake can differentiate chemotherapy sensitive and resistant tumors *in vivo*

We next evaluated the specificity of [18F]FSPG to non-invasively detect drug resistance in living subjects using small animal PET. [18F]FSPG distribution was characterized by high uptake in WT tumors 40 to 60 minutes post injection. Conversely, low tumor-associated radioactivity was measured in size-matched DoxR tumors. Representative static [18F]FSPG maximum-intensity projections (MIPs) are shown in Fig. 4A, with single-slice images displayed in Supplementary Fig. S4, and the corresponding 3-dimensional (3D) movies displayed as movies S1 and S2. Quantification of image-derived [18F]FSPG uptake revealed a 79% decrease in [18F]FSPG uptake in DoxR tumors compared with WT tumors (7.9 ± 0.7 %ID/mL vs. 1.7 ± 0.4 %ID/mL; $n = 5$–6 animals/group; $P < 0.0001$; Fig. 4B). [18F]FSPG tumor retention was above background tissue uptake for both drug-sensitive and drug-resistant tumors, with tumor-to-muscle ratios of 18.8 ± 5.2 and 2.7 ± 1.6 for WT and DoxR, respectively ($n = 5$–6 animals/group; $P < 0.0001$; Supplementary Fig. S5). To understand redox alterations that may underpin this differential [18F]FSPG uptake, the levels of GSH and GSSG were evaluated in snap-frozen tumor samples. In DoxR tumors, GSH was increased 1.6-fold compared with WT, with a nearly 20-fold increase in the ratio of GSSG to GSH measured in the drug-resistant tumors ($n = 3$; $P = 0.0002$; Fig. 4C and D). Western blot analysis revealed xCT, NRF2, GCLC, and glutaminase protein expression remained unchanged between the sensitive and resistant tumors. However, a stabilization in p53 expression was observed in the DoxR tumor samples (Fig. 4E). PEO1, PEO4, and PEO6 cells failed to grow *in vivo*, meaning that we were unable to further corroborate our findings in cell culture using this model.

[18F]FSPG uptake is unchanged in DoxR tumors following therapy

We have shown previously that [18F]FSPG is an early and sensitive marker of drug-induced oxidative stress in A2780 WT tumors (30). To further explore [18F]FSPG as a robust marker

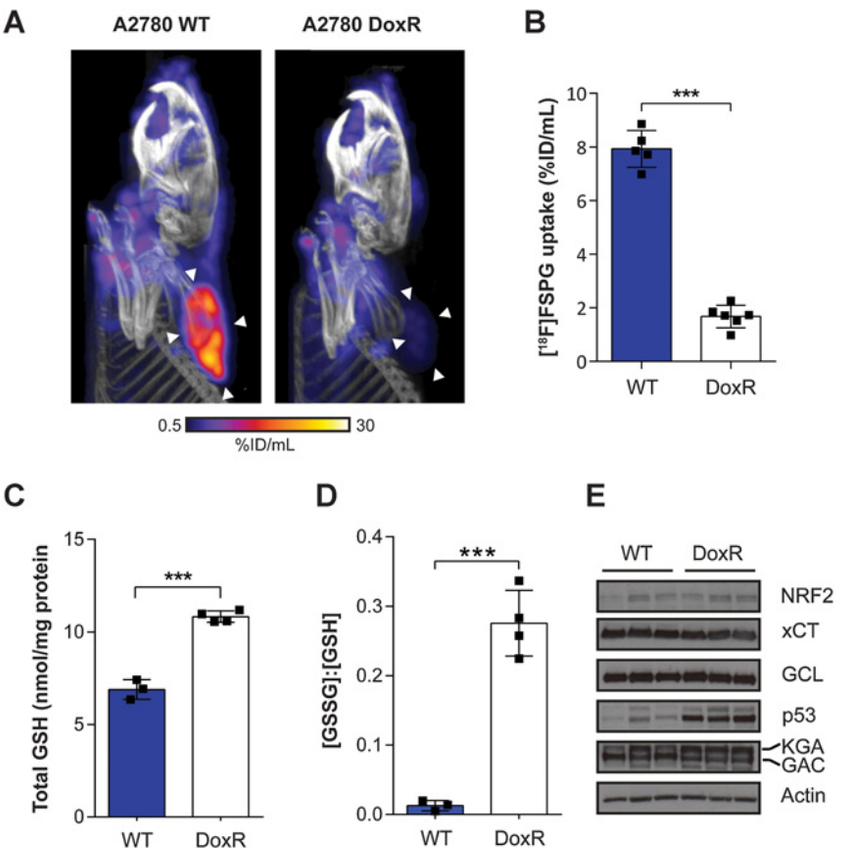

Figure 4.
[18F]FSPG retention is decreased in Doxil-resistant A2780 tumors. **A,** Representative PET/CT maximum intensity projections in WT and DoxR tumor-bearing mice 40 to 60 minutes post-injection. White arrowheads indicate the tumor margins. **B,** Quantification of [18F]FSPG tumor uptake. Total GSH (**C**) and the ratio of GSSG:GSH (**D**) in *ex vivo* tumor samples. ***, $P < 0.001$. Scatter plots represent tumors from separate mice. **E,** Western blot analysis evaluating the expression of proteins involved in cellular antioxidant response and proteins that may influence [18F]FSPG uptake ($n = 3$ xenografts per tumor cell line). Actin was used as a loading control. KGA, kidney-type glutaminase; GAC, glutaminase-C; GCL, glutamate-cysteine ligase.

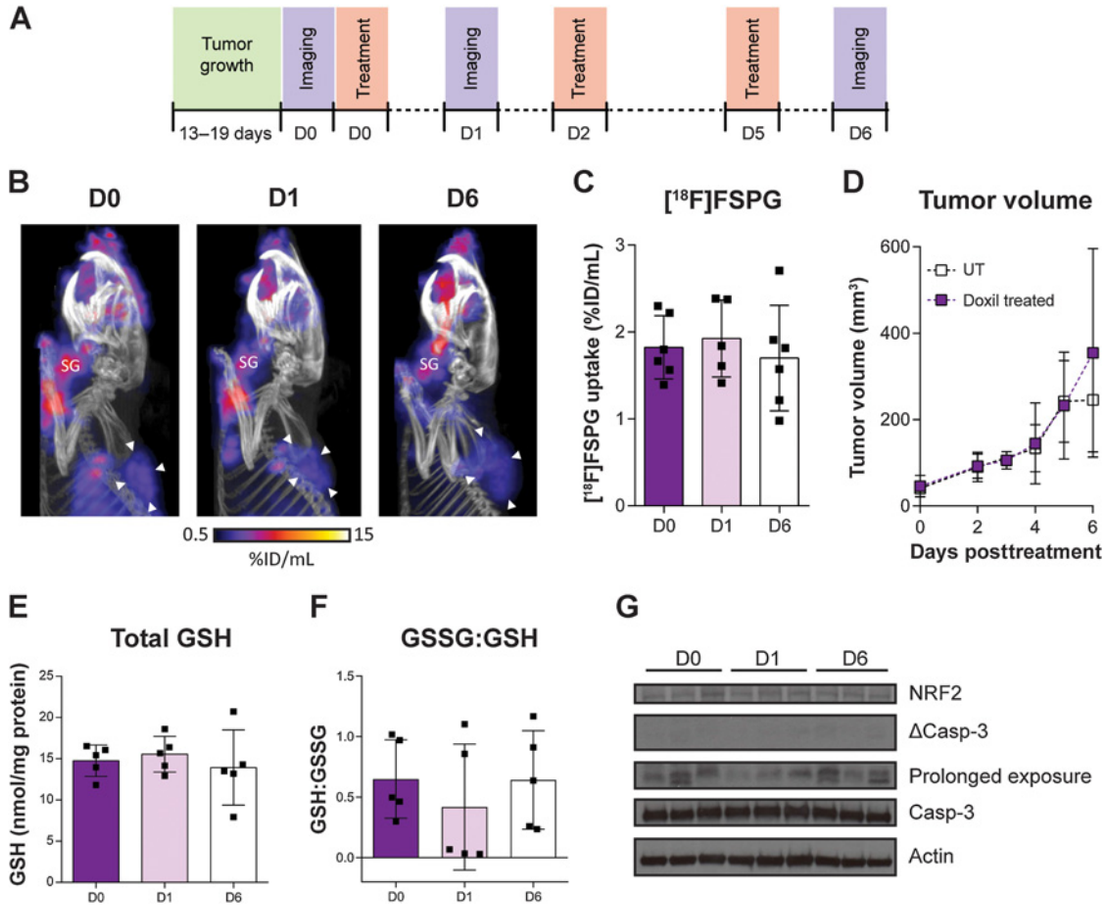

Figure 5.

[^{18}F]FSPG retention is unchanged in A2780 DoxR tumors that fail to respond to therapy. **A,** The treatment and imaging protocol. **B**, Representative PET/CT maximum intensity projections in chemotherapy resistant A2780 DoxR tumor-bearing mice prior to treatment (D0) or following either 24 hours (D1) or 6 days of Doxil treatment (D6). SG, salivary glands. **C**, Quantification of tumor uptake in all 3 treatment groups ($P > 0.05$). **D**, A2780 DoxR tumor growth curves in untreated and drug-treated mice ($P > 0.05$). Total intracellular GSH concentration (**E**) and GSSG:GSH ratio (**F**) from tumor samples taken from untreated and Doxil-treated mice taken immediately following PET imaging ($P > 0.05$). Scatter plots represent tumors from separate mice. **G**, Expression of apoptotic cell death and oxidative stress protein markers. Actin was used as a loading control. Prolonged exposure relates to a 45-minute exposure using a cleaved caspase-3 primary antibody.

of both drug–response and treatment failure, we assessed [^{18}F]FSPG uptake in DoxR tumor xenografts over the same 6-day Doxil treatment time course (Fig. 5A). Representative [^{18}F]FSPG MIPs are shown in Fig. 5B, with single-slice images illustrated in Supplementary Fig. S6, and corresponding 3D movies displayed as movies S3, S4, and S5. Unlike in the A2780 WT tumors (30), there was no significant difference in [^{18}F]FSPG tumor uptake between animals imaged on D0, D1, and D6 (1.8 ± 0.4 %ID/mL, 1.9 ± 0.4 %ID/mL and 1.7 ± 0.6 %ID/mL, respectively; $n = 5$–6 animals/group; $P = 0.94$, D0 vs. D1; and $P = 0.9$, D0 vs. D6; Fig. 5C). Over the course of the experiment, there was also no significant difference in tumor size measured between treated and untreated animals (Fig. 5D), indicating failure of this treatment regimen. Supporting these findings, there was no change in tumor GSH, GSSG:GSH ratio (Fig. 5E and F), markers of oxidative stress (NRF2), or levels of apoptosis following treatment, shown through measurements of caspase 3 cleavage (Fig. 5G).

Discussion

Chemotherapy agents are extensively used for the treatment of many cancers, with the aim to target rapidly growing tissue, often through DNA damage, growth arrest, and the induction of cell death (38). The low therapeutic index of antineoplastic drugs, however, means that relatively small changes in the sensitivity of tumor cells to these agents can be detrimental to patient outcome. The development of novel imaging methods to monitor drug-induced cell death as an indicator of drug efficacy have shown great promise, potentially allowing for a timely intervention following the emergence of drug resistance (39–43). Monitoring response posttreatment, however, is often hampered by difficulties predicting the timescale of response in individual patients. Furthermore, the effective clearance of dying tumor cells by the innate immune system and the high cell turnover in untreated tumors results in cell death being a temporally unstable biomarker of response (44).

The adaptations that occur in cancer cells as a consequence of acquired drug resistance provide ample opportunity for the development of novel, targeted PET radiotracers that have the potential to predict response prior to therapy. Here, we used the redox-sensitive radiotracer, [18F]FSPG, as a surrogate marker of drug resistance. Drug-resistant cancer cells have the ability to maintain a highly reduced intracellular environment to protect themselves from the harmful effects of oxidative stress, thereby conferring treatment resistance (45–47). Using matched drug-sensitive and drug-resistant ovarian cancer cells, we showed that resistance to either cisplatin or doxorubicin corresponded with an increase in tumor antioxidant capacity, defined through the elevation of intracellular GSH and a decrease in ROS. A key component of the tumor's antioxidant system is system x_c^-, which provides cystine for *de novo* GSH biosynthesis. Differential x_c^- activity in drug-resistant versus sensitive A2780 and PEO cells was quantified through measurements of [18F]FSPG cell accumulation, which occurred in the absence of changes in transporter expression. In drug-sensitive cells, [18F]FSPG accumulated to high levels, whereas low intracellular levels were observed in cells resistant to therapy. In comparison, baseline glucose utilization, shown through [18F]FDG uptake, was a poor predictive marker of response.

We have previously shown that the intracellular concentrations of system x_c^- substrates glutamate and cystine mediate [18F]FSPG uptake and retention in A2780 WT tumors (30). In addition, drug-induced oxidative stress in these tumor cells resulted in rapid depletion of intracellular cystine as a consequence of an increase in the rate of *de novo* GSH biosynthesis, which could be imaged by [18F]FSPG PET (30). In all drug-resistant cell lines examined here, intracellular cystine concentrations were substantially decreased compared with drug-sensitive lines, corresponding to large increases in steady-state GSH. In the drug-resistant PEO4 and PEO6 cell lines, where intracellular GSH concentrations were highest of all the cell lines examined, intracellular glutamate—another biosynthetic precursor of GSH—was also significantly decreased compared with the drug-sensitive PEO1 cells. Lowered intracellular glutamate was not observed in the drug-resistant A2780 cell lines, which expressed elevated levels of GLS1, a key metabolic enzyme that catalyzes the conversion of glutamine to glutamate. Through increased glutaminolysis, it is thought that drug-resistant A2780 cells maintained high intracellular glutamate concentrations despite elevated flux into GSH. Conversely, this compensatory mechanism was absent in the resistant PEO4 and PEO6 cell lines which did not upregulate GLS1, which may account for the reduction in intracellular glutamate when compared with PEO1 cells. The PEO4 and PEO6 cell lines did, however, upregulate the expression of the redox-sensitive transcription factor NRF2 which paralleled elevated GCL, its downstream target and the rate-limiting enzyme in GSH biosynthesis. These data suggest there are multiple mechanisms at play that result in elevated de novo GSH biosynthesis and consequent cystine consumption in drug-resistant cells.

Low levels of intracellular cystine present in drug-resistant cells accompanied decreased [18F]FSPG retention compared with their parental drug-sensitive cell line. This decrease in [18F]FSPG accumulation can be understood by considering the mechanism of system x_c^- transport. System x_c^- activity is mediated by the membrane concentration gradients of both glutamate (high intracellular, low extracellular) and cystine (low intracellular, high extracellular; ref. 48). Depletion of intracellular cystine acts to increase system x_c^--mediated cystine uptake into the cell, with a corresponding increase in glutamate efflux. As [18F]FSPG can replace glutamate as an exchange partner with cystine, lowered intracellular [18F]FSPG measured in drug resistant tumors may be a consequence of elevated radiotracer efflux from the cell. Additionally, increased cystine uptake may alternatively lead to higher occupancy of the transporter by the natural substrate and therefore lower [18F]FSPG uptake. Furthermore, a decrease in intracellular glutamate, as observed in PEO4 and PEO6 cells, will lower the rate of glutamate efflux, thereby reducing the rate of both cystine and [18F]FSPG uptake. Taken together, a depletion of either intracellular glutamate or cystine is predicted to reduce overall [18F]FSPG accumulation, as shown in this study. A schematic illustrating the putative relationship between the intracellular-to-extracellular concentration gradients of cystine and glutamate, [18F]FSPG tumor retention, and drug resistance is shown in Fig. 6.

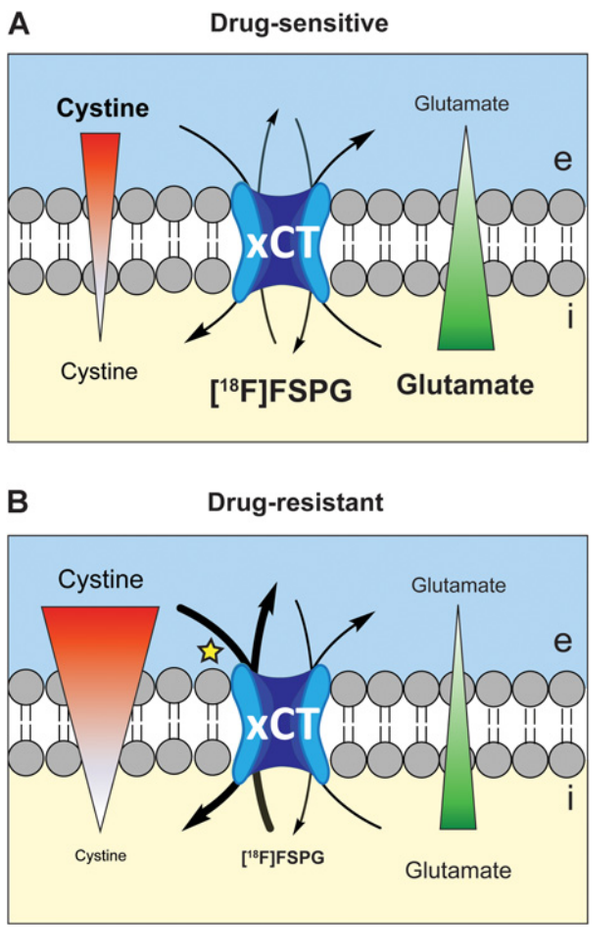

Figure 6.

Schematic illustrating the proposed mechanism of [18F]FSPG accumulation in sensitive and drug-resistant tumors. Changes in the concentration gradients of either cystine or glutamate in drug-sensitive (**A**) and drug-resistant (**B**) tumor cells are predicted to cause alterations in [18F]FSPG tumor retention. A decrease in intracellular cystine leads to an increase in the concentration gradient across the membrane, expected to result in increased efflux of [18F]FSPG in exchange for increased influx of extracellular cystine. Alternatively, decreased uptake in drug-resistant tumors may be a consequence of increased competition between cystine and [18F]FSPG at the site of the transporter (denoted by the yellow star). Red and green triangles represent the concentration gradients of cystine and glutamate, respectively. e, extracellular; i, intracellular.

Corroborating our findings in culture, tumor-associated [^{18}F]FSPG was decreased in drug-resistant A2780 DoxR xenografts when compared with drug-sensitive WT tumors, which was also independent of any changes in xCT expression. In the drug-resistant DoxR tumors, we observed an elevation in total tumor GSH and 21-fold increase in GSSG:GSH ratio when compared with WT—indicating an adaptive mechanism to maintain a decreased intracellular environment through upregulation of this key antioxidant pathway. This reducing environment facilitates the protection against ROS-induced cell death, subsequently lowering drug-induced toxicity and resulting in drug resistance. We have previously shown that [^{18}F]FSPG uptake is an early and sensitive marker of treatment response in doxorubicin-sensitive A2780 WT tumors (30). WT tumors were treated with Doxil over the same 6-day treatment time course described here (Fig. 5A), with [^{18}F]FSPG retention decreased by a significant 42% 24 hours post therapy. In these drug-sensitive WT tumors, a reduction in [^{18}F]FSPG coincided with a depletion in tumor GSH but occurred prior to measurable changes in tumor volume, which became evident 4 days after the initial round of treatment (30). Given that DoxR tumors upregulate the antioxidant GSH and maintain low levels of ROS, we asked if this reducing environment was sufficient to protect these tumors from oxidizing Doxil treatment and whether [^{18}F]FSPG PET could monitor drug–response (or its absence) posttherapy. In these resistant tumors, 3 doses of Doxil therapy over the 6-day treatment time course did not induce caspase-3 activation, with treatment unable to alter tumor growth *in vivo*. Treatment failure corresponded with an absence of changes in total GSH and the GSSG:GSH ratio from baseline. Importantly, no differences in [^{18}F]FSPG tumor uptake were measured between treatment groups, indicating that [^{18}F]FSPG uptake cannot only be used to predict drug resistance, but monitor treatment response, and indeed treatment failure.

The non-invasive imaging of chemotherapy-resistant xenografts with [^{18}F]FSPG holds some limitations. The tumoral heterogeneity in human ovarian cancer results in multiple highly complex mechanisms of chemotherapy resistance, as previously reported (49, 50). We have shown here that [^{18}F]FSPG can be used as a non-invasive method to identify chemotherapy-resistance tumors through measurement of their antioxidant capacity. Other well-established mechanisms of resistance include the upregulation of the ABC efflux pumps (37). In the cell lines tested here, there was no clear pattern of ABC transporter upregulation in the drug-resistant cells, with only A2780 DoxR cells expressing detectable levels of ABCB1 and ABCC2. In DoxR cells, elevated GSH observed (Fig. 1F) may be a requirement for ABC transporter-mediated efflux of doxorubicin–GSH conjugates. Upregulation of *de novo* GSH synthesis as a consequence of ABC transporter expression could presumably affect intracellular cystine levels and therefore reduce [^{18}F]FSPG retention. From this study, however, it is unclear whether the detection of resistant tumors using mechanisms to overcome insult with chemotherapeutic drugs that do not cause changes in the cellular antioxidant response will cause a change in tumor [^{18}F]FSPG uptake. Moreover, it is expected that metabolic adaptation in tumors, such as altered anaplerotic flux, may alter [^{18}F]FSPG uptake irrespective of the resistance-status of the cells. Regarding clinical utility, it may therefore be necessary to acquire a baseline scan for each patient upon diagnosis, with follow-up [^{18}F]FSPG scans performed upon relapse. Importantly, however, as [^{18}F]FSPG has already been examined in human clinical trials, there are few barriers to the use of [^{18}F]FSPG as a predictive marker of drug resistance in patients.

Conclusion

Here, we have shown that [^{18}F]FSPG uptake is uniquely sensitive to the upregulated antioxidant pathways present in drug-resistant human ovarian tumors. In the drug-resistant lines, low [^{18}F]FSPG uptake corresponded with decreased ROS and higher baseline GSH concentrations in comparison to drug-sensitive tumors. [^{18}F]FSPG may therefore enable the identification of patients with ovarian cancer that are refractory to the standard of care, as well as monitor their response posttreatment. Transferal of drug-resistant patients to alternative therapies has the potential to increase tumor response and patient survival. In addition, [^{18}F]FSPG PET holds great potential for the prediction of drug sensitivity in a range of other malignancies that share the same underlying mechanisms of resistance.

Disclosure of Potential Conflicts of Interest

D. Hochhauser reports receiving commercial research grants from Merck Serono. N. Koglin holds ownership interest (including patents) in FSPG. T.H. Witney reports receiving commercial research grants from Life Molecular Imaging GmbH, and is a consultant/advisory board member for CellSight Technologies, Inc. No potential conflicts of interest were disclosed by the other authors.

Authors' Contributions

Conception and design: P.N. McCormick, D. Hochhauser, T.H. Witney
Development of methodology: H.E. Greenwood, P.N. McCormick, T. Gendron, K. Sander, M.F. Lythgoe, D. Hochhauser, T.H. Witney
Acquisition of data (provided animals, acquired and managed patients, provided facilities, etc.): H.E. Greenwood, P.N. McCormick, T. Gendron, O.D.K. Maddocks, T. Zhang, E. Årstad, T.H. Witney
Analysis and interpretation of data (e.g., statistical analysis, biostatistics, computational analysis): H.E. Greenwood, P.N. McCormick, O.D.K. Maddocks, T. Zhang, N. Koglin, M.F. Lythgoe, D. Hochhauser, T.H. Witney
Writing, review, and/or revision of the manuscript: H.E. Greenwood, T. Gendron, M. Glaser, K. Sander, N. Koglin, M.F. Lythgoe, D. Hochhauser, T.H. Witney
Administrative, technical, or material support (i.e., reporting or organizing data, constructing databases): M. Glaser, K. Sander, T.H. Witney
Study supervision: D. Hochhauser, T.H. Witney
Other (radiosynthesis): R. Pereira

Acknowledgments

The authors would like to thank Stephen Patrick, May Zaw-Thin, and Andrew Stephens for insightful scientific discussions and William Day for help with flow cytometric experiments. This study was funded through a Wellcome Trust and Royal Society Sir Henry Dale Fellowship (107610/Z/15/Z) and the Cancer Research UK-UCL Centre Development Award (C416/A18088) to Timothy Witney, the CRUK & EPSRC Comprehensive Cancer Imaging Centre at KCL & UCL (C1519/A16463) to Erik Årstad, and financial support from Life Molecular Imaging GmbH (formerly Piramal Imaging) to Timothy Witney. UCL radiochemistry is funded in-part by the Department of Health's NIHR Biomedical Research Centres funding scheme. Oliver Maddocks and Tong Zhang are supported by CRUK Career Development Fellowship C53309/A19702.

The costs of publication of this article were defrayed in part by the payment of page charges. This article must therefore be hereby marked *advertisement* in accordance with 18 U.S.C. Section 1734 solely to indicate this fact.

Received October 19, 2018; revised December 18, 2018; accepted January 14, 2019; published first January 16, 2019.

References

1. 2012 Ovarian cancer statistics In Cancer Research UK. <http://www.cancerresearchuk.org/health-professional/cancer-statistics/statistics-by-cancer-type/ovarian-cancer/survival#heading-Zero>.
2. Chen M, Jin Y, Bi Y, Yin J, Wang Y, Pan L. A survival analysis comparing women with ovarian low-grade serous carcinoma to those with high-grade histology. Oncotargets Ther 2014;7:1891–9.
3. Wiedemeyer WR, Beach JA, Karlan BY. Reversing platinum resistance in high-grade serous ovarian carcinoma: targeting BRCA and the homologous recombination system. Front Oncol 2014;4:34. doi: 10.3389/fonc.2014.00034.
4. Parmar MKB, Ledermann JA, Colombo N, du Bois A, Delaloye JF, Kristensen GB, et al. Paclitaxel plus platinum-based chemotherapy versus conventional platinum-based chemotherapy in women with relapsed ovarian cancer: the ICON4/AGO-OVAR-2.2 trial. Lancet 2003;361:2099–106.
5. Pujade-Lauraine E, Alexandre J. Update of randomized trials in recurrent disease. Ann Oncol 2011;22 Suppl 8:viii61–4.
6. Markman M RR, Hakes T, Reichman B, Hoskins W, Rubin S, Jones W, et al. Second-line platinum therapy in patients with ovarian cancer previously treated with cisplatin. J Clin Oncol 1991;9:389–93.
7. Colombo N, Gore M. Treatment of recurrent ovarian cancer relapsing 6–12 months post platinum-based chemotherapy. Crit Rev Oncol Hemat 2007;64:129–38.
8. Mullany LK, Richards JS. Minireview: animal models and mechanisms of ovarian cancer development. Endocrinology 2012;153:1585–92.
9. Clemens MR, Ladner C, Ehninger G, Einsele H, Renn W, Buhler E, et al. Plasma vitamin E and beta-carotene concentrations during radiochemotherapy preceding bone marrow transplantation. Am J Clin Nutr 1990;51:216–9.
10. Durken M, Agbenu J, Finckh B, Hubner C, Pichlmeier U, Zeller W, et al. Deteriorating free radical-trapping capacity and antioxidant status in plasma during bone marrow transplantation. Bone Marrow Transpl 1995;15:757–62.
11. Erhola M, Kellokumpu-Lehtinen P, Metsa-Ketela T, Alanko K, Nieminen MM. Effects of anthracyclin-based chemotherapy on total plasma antioxidant capacity in small cell lung cancer patients. Free Radic Biol Med 1996;21:383–90.
12. Faber M, Coudray C, Hida H, Mousseau M, Favier A. Lipid peroxidation products, and vitamin and trace element status in patients with cancer before and after chemotherapy, including adriamycin. A preliminary study. Biol Trace Elem Res 1995;47:117–23.
13. Faure H, Coudray C, Mousseau M, Ducros V, Douki T, Bianchini F, et al. 5-Hydroxymethyluracil excretion, plasma TBARS and plasma antioxidant vitamins in adriamycin-treated patients. Free Radic Biol Med 1996;20:979–83.
14. Ladner C, Ehninger G, Gey KF, Clemens MR. Effect of etoposide (VP16-213) on lipid peroxidation and antioxidant status in a high-dose radiochemotherapy regimen. Cancer Chemother Pharmacol 1989;25:210–2.
15. Look MP, Musch E. Lipid peroxides in the polychemotherapy of cancer patients. Chemotherapy 1994;40:8–15.
16. Sangeetha P, Das UN, Koratkar R, Suryaprabha P. Increase in free radical generation and lipid peroxidation following chemotherapy in patients with cancer. Free Radic Biol Med 1990;8:15–9.
17. Weijl NI, Hopman GD, Wipkink-Bakker A, Lentjes EG, Berger HM, Cleton FJ, et al. Cisplatin combination chemotherapy induces a fall in plasma antioxidants of cancer patients. Ann Oncol 1998;9:1331–7.
18. Balendiran GK, Dabur R, Fraser D. The role of glutathione in cancer. Cell Biochem Funct 2004;22:343–52.
19. Britten RA, Green JA, Warenius HM. Cellular glutathione (GSH) and glutathione S-transferase (GST) activity in human ovarian tumor biopsies following exposure to alkylating agents. Int J Radiat Oncol Biol Phys 1992;24:527–31.
20. Calvert P, Yao K-S, Hamilton TC, O'Dwyer PJ. Clinical studies of reversal of drug resistance based on glutathione. Chem-Biol Interact 1998;111–112:213–24.
21. Lewis AD, Duran GE, Lau DH, Sikic BI. Sensitization of drug resistant human ovarian cancer cells to cyanomorpholino doxorubicin (MRA-CN) by modulation of glutathione metabolism. Int J Radiat Oncol Biol Phys 1992;22:821–4.
22. Ozols RF, Louie KG, Plowman J, Behrens BC, Fine RL, Dykes D, et al. Enhanced melphalan cytotoxicity in human ovarian cancer in vitro and in tumor-bearing nude mice by buthionine sulfoximine depletion of glutathione. Biochem Pharmacol 1987;36:147–53.
23. Pan B, Yao KS, Monia BP, Dean NM, McKay RA, Hamilton TC, et al. Reversal of cisplatin resistance in human ovarian cancer cell lines by a c-jun antisense oligodeoxynucleotide (ISIS 10582): evidence for the role of transcription factor overexpression in determining resistant phenotype. Biochem Pharmacol 2002;63:1699–707.
24. Bridges RJ, Natale NR, Patel SA. System x(c)(-) cystine/glutamate antiporter: an update on molecular pharmacology and roles within the CNS. Br J of Pharmacol 2012;165:20–34.
25. Tian M, Guo F, Sun Y, Zhang W, Miao F, Liu Y, et al. A fluorescent probe for intracellular cysteine overcoming the interference by glutathione. Org Biomol Chem 2014;12:6128–33.
26. Koglin N, Mueller A, Berndt M, Schmitt-Willich H, Toschi L, Stephens AW, et al. Specific PET imaging of xc- transporter activity using a 18F-labeled glutamate derivative reveals a dominant pathway in tumor metabolism. Clin Cancer Res 2011;17:6000–11.
27. Mittra ES, Koglin N, Mosci C, Kumar M, Hoehne A, Keu KV, et al. Pilot Preclinical and Clinical Evaluation of (4S)-4-(3-[18F]Fluoropropyl)-L-Glutamate (18F-FSPG) for PET/CT imaging of intracranial malignancies. PLoS One 2016;11:e0148628.
28. Baek S, Choi CM, Ahn SH, Lee JW, Gong G, Ryu JS, et al. Exploratory clinical trial of (4S)-4-(3-[18F]fluoropropyl)-L-glutamate for imaging xC- transporter using positron emission tomography in patients with non-small cell lung or breast cancer. Clin Cancer Res 2012;18:5427–37.
29. Kavanaugh G, Williams J, Morris AS, Nickels ML, Walker R, Koglin N, et al. Utility of [18F]FSPG PET to image hepatocellular carcinoma: first clinical evaluation in a US population. Mol Imaging Biol 2016;18:924–34.
30. McCormick PN, Greenwood HE, Glaser M, Maddocks ODK, Gendron T Sander K, et al. Assessment of tumor redox status through (S)-4-(3-[18F]fluoropropyl)-L-glutamic acid positron emission tomography imaging of system xc- activity. Cancer Res 2019;79:853–63.
31. Witney TH, Kettunen MI, Day SE, Hu D-e, Neves AA, Gallagher FA, et al. A comparison between radiolabeled fluorodeoxyglucose uptake and hyperpolarized 13C-Labeled pyruvate utilization as methods for detecting tumor response to treatment. Neoplasia 2009;11:574–582.
32. Witney TH, James ML, Shen B, Chang E, Pohling C, Arksey N, et al. PET imaging of tumor glycolysis downstream of hexokinase through noninvasive measurement of pyruvate kinase M2. Sci Transl Med 2015;7:310ra169-310ra169.
33. Louie KG, Behrens BC, Kinsella TJ, Hamilton TC, Grotzinger KR, McKoy WM, et al. Radiation survival parameters of antineoplastic drug-sensitive and -resistant human ovarian cancer cell lines and their modification by buthionine sulfoximine. Cancer Res 1985;45:2110–5.
34. Behrens BC, Hamilton TC, Masuda H, Grotzinger KR, Whang-Peng J, Louie KG, et al. Characterization of a cis-diamminedichloroplatinum(II)-resistant human ovarian cancer cell line and its use in evaluation of platinum analogues. Cancer Res 1987;47:414–8.
35. Langdon SP, Lawrie SS, Hay FG, Hawkes MM, McDonald A, Hayward IP, et al. Characterization and properties of nine human ovarian adenocarcinoma cell lines. Cancer Res 1988;48:6166–72.
36. Analysis of Drug Resistant Properties of A2780 Ovarian Cancer Cell Lines Using Label-Free Automated Microscopy (IncuCyte ZOOM) Public Health England 2016.
37. Gottesman MM, Fojo T, Bates SE. Multidrug resistance in cancer: role of ATP–dependent transporters. Nat Rev Cancer 2002;2:48–58.
38. Ho Y-P, Au-Yeung SCF, To KKW. Platinum-based anticancer agents: Innovative design strategies and biological perspectives. Med Res Rev 2003;23:633–55.
39. Witney TH, Kettunen MI, Hu De, Gallagher FA, Bohndiek SE, Napolitano R, et al. Detecting treatment response in a model of human breast adenocarcinoma using hyperpolarised [1-13C]pyruvate and [1,4-13C2]fumarate. Br J Cancer 2010;103:1400–6.
40. Witney TH, Hoehne A, Reeves R, Ilovich O, Namavari M, Shen B, et al. A systematic comparison of 18F-C-SNAT to established radiotracer imaging

agents for the detection of tumor response to treatment. Clin Cancer Res 2015;27:3896–905.
41. Witney TH, Fortt RR, Aboagye EO. Preclinical Assessment of Carboplatin Treatment Efficacy in Lung Cancer by 18F-ICMT-11-Positron Emission Tomography. PLOS ONE 2014;9:e91694.
42. Alam IS, Neves AA, Witney TH, Boren J, Brindle KM. Comparison of the C2A Domain of Synaptotagmin-I and Annexin-V As Probes for Detecting Cell Death. Bioconjugate Chem 2010;21:884–91.
43. Palmieri L, Elvas F, Vangestel C, Pak K, Gray B, Stroobants S, et al. [(99m) Tc]duramycin for cell death imaging: Impact of kit formulation, purification and species difference. Nucl Med Biol 2018;56:1–9.
44. Lauber K, Ernst A, Orth M, Herrmann M, Belka C. Dying cell clearance and its impact on the outcome of tumor radiotherapy. Front Oncol 2012;2:116. doi: 10.3389/fonc.2012.00116.
45. Ballatori N, Krance SM, Notenboom S, Shi S, Tieu K, Hammond CL. Glutathione dysregulation and the etiology and progression of human diseases. J Biol Chem 2009;390:191–214.
46. Godwin AK, Meister A, O'Dwyer PJ, Huang CS, Hamilton TC, Anderson ME. High resistance to cisplatin in human ovarian cancer cell lines is associated with marked increase of glutathione synthesis. Proc Natl Acad Sci 1992;89:3070–4.
47. Meijer C, Mulder NH, Timmer-Bosscha H, Sluiter WJ, Meersma GJ, de Vries EGE. Relationship of Cellular Glutathione to the Cytotoxicity and Resistance of Seven Platinum Compounds. Cancer Res 1992;52: 6885–9.
48. Bannai S, Ishii T. A novel function of glutamine in cell culture: utilization of glutamine for the uptake of cystine in human fibroblasts. J Cell Physiol 1988;137:360–6.
49. Perez RP, Hamilton TC, Ozols RF, Young RC. Mechanisms and modulation of resistance to chemotherapy in ovarian cancer. Cancer 1993;71(S4): 1571–80.
50. Rabik CA, Dolan ME. Molecular Mechanisms of Resistance and Toxicity Associated with Platinating Agents. Cancer treat rev 2007; 33:9–23.